ACS APPLIED MATERIALS & INTERFACES

Letter

www.acsami.org

Enhancement of Visible-Light Photocatalysis by Coupling with Narrow-Band-Gap Semiconductor: A Case Study on Bi_2S_3/Bi_2WO_6

Zhijie Zhang, Wenzhong Wang,* Lu Wang, and Songmei Sun

State Key Laboratory of High Performance Ceramics and Superfine Microstructures, Shanghai Institute of Ceramics, Chinese Academy of Sciences, 1295 Dingxi Road, Shanghai 200050, PR China

ABSTRACT: To overcome the drawback of low photocatalytic efficiency brought by electron−hole recombination and narrow photoresponse range, we designed a novel Bi_2S_3/Bi_2WO_6 composite photocatalyst. The composite possesses a wide photoabsorption until 800 nm, which occupies nearly the whole range of the visible light. Compared with bare Bi_2WO_6, the Bi_2S_3/Bi_2WO_6 composite exhibits significantly enhanced photocatalytic activity for phenol degradation under visible light irradiation. On the basis of the calculated energy band positions, the mechanism of enhanced photocatalytic activity was proposed. The present study provides a new strategy to design composite materials with enhanced photocatalytic performance.

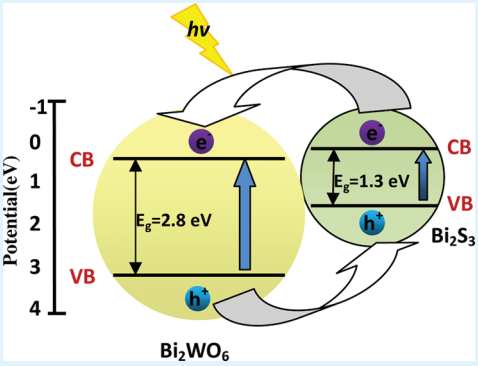

KEYWORDS: *Bi_2S_3/Bi_2WO_6 composite, photocatalysis, heterojunction, phenol*

INTRODUCTION

Photocatalysts for organic pollutants degradation and hydrogen generation from water using solar light energy has attracted increasing interest in the past years due to the growing environment concerns and the energy demand.[1−5] Because the photocatalytic process involves the generation of charge carriers such as electrons and holes induced by light, an ideal photocatalyst should have both a wide photoabsorption range and a low recombination rate of the photogenerated charge carriers. Therefore, it is necessary to develop effective ways to improve the charge separation efficiency and extend the spectral responsive range. The idea of forming a heterojunction structure between a photocatalyst and a narrow bandgap semiconductor with matched band potentials may provide such a way to address these two issues.[6−10]

As one of the simplest Aurivillius oxides with layered structure, Bi_2WO_6 is special for its good photocatalytic performance under visible light irradiation.[11−15] Bare Bi_2WO_6 presents photoabsorption properties from UV light to visible light with wavelength of shorter than ca. 450 nm,[16,17] which occupies a small part of the solar spectrum. Moreover, the rapid recombination of photoinduced electron−hole pairs seriously limits the energy-conversion efficiency. To broaden the range of visible-light photoresponse and promote the separation of photogenerated carriers of Bi_2WO_6, we intended to design a composite photocatalyst by coupling Bi_2WO_6 with a narrow bandgap semiconductor with matched band potentials. The well-established heterojunction structure could be employed to restrict the recombination of the charge carriers and enhance the quantum yield.[18] The electrons excited by visible light can be transferred to Bi_2WO_6 from the narrow bandgap semiconductor, which favors the charge separation and also improves the visible-light photocatalytic activity of the heterostructure dramatically.

Bismuth sulfide (Bi_2S_3) with a narrow bandgap (~1.3 eV) can be a good candidate semiconductor.[19−21] It has been used as electrochemical hydrogen storage, hydrogen sensors, biomolecule detection, X-ray computed tomography imaging, and photoresponsive materials.[22−26] More recentely, it has been acted as a sensitizer due to its ability to absorb a large part of visible light up to 800 nm.[27,28] To investigate the relative energy band positions, we calculated the band positions of Bi_2S_3 and Bi_2WO_6 and found that the conduction band of Bi_2S_3 is less anodic than the corresponding band of Bi_2WO_6 and the valence band of this sensitizer is more cathodic than that of Bi_2WO_6. The calculated results indicate that it is possible the formation of Bi_2S_3/Bi_2WO_6 heterojunction will be advantageous for the separation and transportation of charge carriers. Therefore the Bi_2S_3/Bi_2WO_6 composite could have a good photocatalytic performance under visible light.

In this study, the Bi_2S_3/Bi_2WO_6 composite was prepared by a hydrothermal method for the first time. The photoactivity evaluation, via the photocatalytic degradation of phenol under visible light, demonstrated that the Bi_2S_3/Bi_2WO_6 composite exhibits much enhanced photocatalytic activity than bare Bi_2WO_6. On the basis of the calculated energy band positions, the mechanism of enhanced photocatalytic activity for the Bi_2S_3/Bi_2WO_6 composite was also discussed in detail.

Received: December 5, 2011
Accepted: January 16, 2012
Published: January 16, 2012

EXPERIMENTAL SECTION

Preparation of the Composite Photocatalysts. All the reagents were of analytical purity and were used as received from Shanghai Chemical Company. A typical synthetic procedure toward the Bi_2S_3/Bi_2WO_6 composite can be described briefly as follows: a mixture of thiourea and $Na_2WO_4{\cdot}2H_2O$ was dissolved in 30 mL deionized water under constant stirring. Meanwhile, $Bi(NO_3)_3{\cdot}5H_2O$ was dissolved in diluted nitric acid to form a clear solution. After that, these two solutions were mixed together and the pH of this mixed solution was adjusted to 7 using given amounts of NaOH solution. After being stirred for 2 h, the suspension was transferred into a 50 mL Teflon-lined stainless steel autoclave up to 80% of the total volume. The autoclave was heated at 160 °C for 24 h, and then cooled to room temperature naturally. The resulting products were separated by filtration, washed with deionized water and absolute alcohol for several times, and then dried at 60 °C for 12 h. For comparison, bare Bi_2WO_6 was also prepared by the hydrothermal method under the same conditions as mentioned above.

Characterization. The phase and composition of the as-prepared samples were measured by X-ray diffraction (XRD) studies using an X-ray diffractometer with Cu Kα radiation under 40 kV and 100 mA and with the 2θ ranging from 20 to 70° (Rigaku, Japan). The morphologies and microstructures of the as-prepared samples were investigated by Transmission Electron Microscopy (TEM) (JEOL JEM-2100F, accelerating voltage 200 kV). UV−vis diffuse reflectance spectra (DRS) of the samples were recorded with an UV−vis spectrophotometer (Hitachi U−3010) using $BaSO_4$ as reference. The photoluminescene (PL) measurements were carried out on a Fluorolog-3 fluorescence spectrophotometer (Jobin Yvon, France) at room temperature. Total organic carbon (TOC) analysis was carried out with an elementar liqui TOC II analyzer.

Photocatalytic Test. The photocatalytic activities of the Bi_2S_3/Bi_2WO_6 composite photocatalyst were evaluated by photocatalytic degradation of a colorless model pollutant, phenol under visible light. A 500 W Xe lamp with a 420 nm cutoff filter was used as the light source. The experiments were performed at room temperature as follows: 0.05 g of photocatalyst was added into 50 mL phenol solution (20 mg/L). Prior to irradiation, the suspensions were magnetically stirred for an hour in the dark to ensure the adsorption/desorption equilibrium between photocatalyst powders and phenol. At given time intervals, 3 mL suspensions were sampled and centrifuged to remove the photocatalyst powders. The concentration of phenol was analyzed through a UV−vis spectrophotometer (Hitachi U−3010) by recording the variations of the absorption band maximum (269 nm).

RESULTS AND DISCUSSION

The crystal structure of the products was investigated by the powder X-ray diffraction (XRD) method, as shown in Figure 1. The XRD pattern of Figure 1A indicates that all the peaks are readily indexed to the orthorhombic phase of Bi_2WO_6 according to the JCPDS card no. 39−0256. The diffraction profile of Figure 1B showed that the composite was composed of orthorhombic Bi_2WO_6 (JCPDS 39−0256) and orthorhombic Bi_2S_3 (JCPDS 84−0279). No characteristic peaks of any impurities are detected in the patterns.

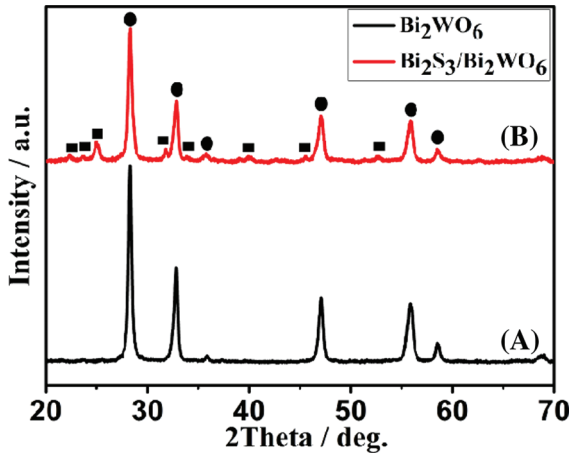

Figure 1. XRD patterns of the products. Squares (■) and circles (●) indicate the representative peaks of Bi_2S_3 and Bi_2WO_6, respectively.

The morphology and microstructure of the Bi_2S_3/Bi_2WO_6 composite were revealed by the transmission electron microscope (TEM) images. The TEM image in Figure 2(A) shows

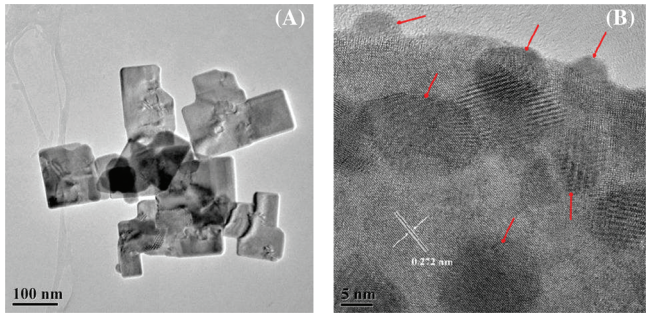

Figure 2. (A) TEM image of the Bi_2S_3/Bi_2WO_6 composite; (B) high-resolution TEM image of the Bi_2S_3/Bi_2WO_6 composite, red arrows indicate the Bi_2S_3 nanoparticles.

that the composite possesses a two-dimensional plate-like structure with lateral sizes of 100−200 nm, which agrees well with the microstructure of bare Bi_2WO_6 in our previous reports.[29,30] However, the high-resolution TEM (HRTEM) in Figure 2(B) shows that some tiny nanocrystals with sizes of 5−10 nm are inlaid in the plate matrix. The clear lattice spacing of the plate matrix is about 0.272 nm, which is consistent with the *d*-spacing (0.272 nm) of the [2 0 0] reflection of Bi_2WO_6. In the synthetic process, Bi_2WO_6 precipitate formed first. Then thiourea decomposed during the hydrothermal process to generate S^{2-} ions. It is known that compound with high-solubility can be converted into another compound with low solubility under the driving force of solubility difference in solution. Because the solubility of Bi_2S_3 is extremely low (K_{sp} = 1×10^{-97}), Bi_2WO_6 can be easily converted into Bi_2S_3 when it exchanges anion with S^{2-} ions in solution. So some areas of Bi_2WO_6 nanoplate were eroded to generate Bi_2S_3 nanocrystals inlaid in the plate matrix. The formation of the intimate junction structure is significant which may promote the charge separation to achieve high photocatalytic activity in the coupling system.

The quantitative chemical composition of the Bi_2S_3/Bi_2WO_6 composite was analyzed by X-ray fluorescence spectroscopy (XRF). The results demonstrated that the molar percentage of

dx.doi.org/10.1021/am2017199 | ACS Appl. Mater. Interfaces 2012, 4, 593−597

Bi:W:S is 56:21:25. In other words, the fraction of Bi atoms in the form of sulphide in the nanocomposite is 28.4%.

The UV−vis diffuse reflection spectrum (DRS) of the as-prepared samples was shown in Figure 3. According to the

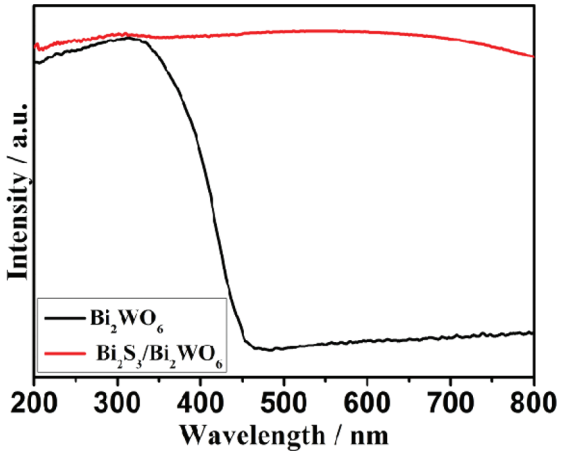

Figure 3. UV−vis diffuse reflectance spectra of the as-prepared samples.

spectrum, bare Bi_2WO_6 sample presents the photoresponse property from the UV light region to visible light until 450 nm. Compared with bare Bi_2WO_6, the light absorption ability of the composite is significantly enhanced after Bi_2S_3 was introduced, which has strong absorption in nearly the whole range of visible light. This can be attributed to the small band gap and large absorption coefficient of Bi_2S_3. Taking into account the efficient use of visible light in a large part of the solar spectrum, we believe that this photocatalyst, with its long wavelength absorption band, is an attractive photocatalyst for pollutant degradation.

Because photoluminescence (PL) emission mainly results from the recombination of free carriers, PL spectra is a useful technique to survey the separation efficiency of the photogenerated charge carriers in a semiconductor.[31] The higher the PL intensity, the bigger probability the charge carrier recombination.[32] The comparison of PL spectra (excited at 300 nm) of bare Bi_2WO_6 and the Bi_2S_3/Bi_2WO_6 composite at room temperature is shown in Figure 4. Bi_2WO_6 has a broad

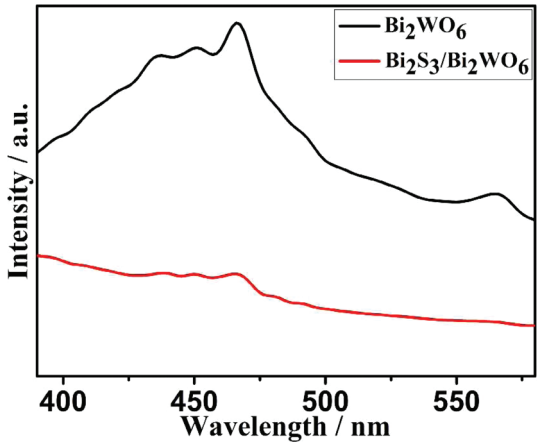

Figure 4. Room-temperature photoluminescence (PL) spectrum of the as-prepared samples (λ_{Ex} = 300 nm).

blue-green emission peak. The strongest blue emitting peaks at ca. 460 nm is attributed to the intrinsic luminescence of Bi_2WO_6, which originates from the charge-transfer transitions between the hybrid orbital of Bi_{6s} and O_{2p} (VB) to the empty W_{5d} orbital (CB) in the WO_6^{2-} complex.[33] It was found that PL emission intensity of the Bi_2S_3/Bi_2WO_6 composite was dramatically weakened compared with that of bare Bi_2WO_6, which clearly indicates that the recombination of photogenerated charge carriers between the hybrid orbital of Bi_{6s} and O_{2p} (VB) to the empty W_{5d} orbital is greatly inhibited by the heterojunction nanostructure. In other words, the coupling of Bi_2WO_6 and Bi_2S_3 is helpful to separate the photogenerated charge carriers.

The photocatalytic activity of the Bi_2S_3/Bi_2WO_6 composite was tested and compared with bare Bi_2WO_6 under visible-light irradiation. As a typical colorless contaminant, phenol was selected as the model pollutant instead of dyes so as to exclude the sensitization effect. Figure 5A shows the photodegradation

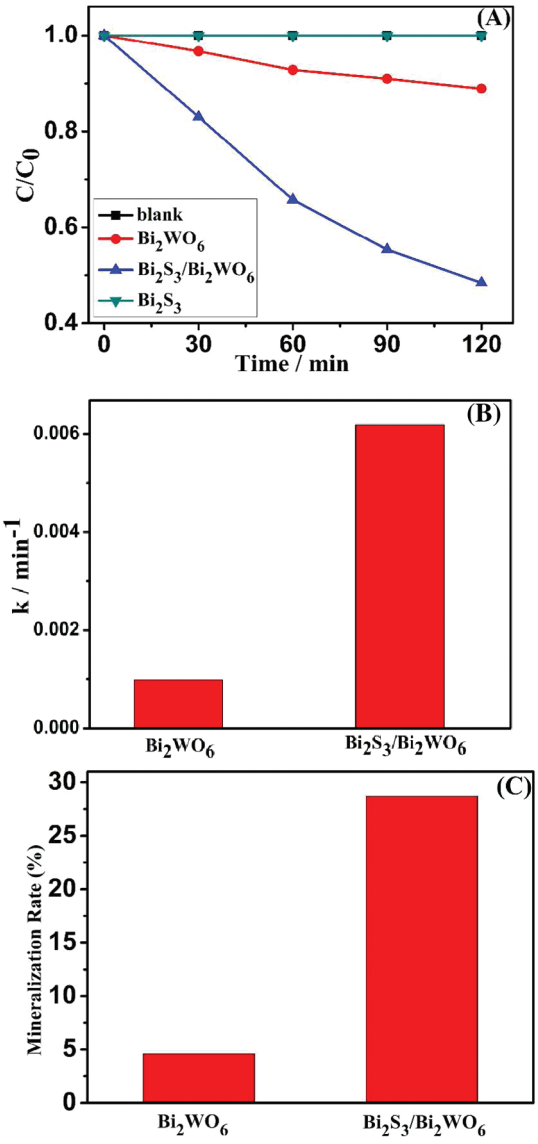

Figure 5. (A) Degradation efficiency of phenol as a function of time by the as-prepared samples under visible light irradiation; (B) Comparison of rate constant *k*. (C) Comparison of mineralization rate of phenol by the as-prepared samples.

dx.doi.org/10.1021/am2017199 | ACS Appl. Mater. Interfaces 2012, 4, 593−597

rate of phenol as a function of time, where C was the concentration of phenol after irradiation and C_0 was the concentration after the adsorption equilibrium on the photocatalyst particles before irradiation. Blank tests (phenol solution without any photocatalyst) under visible light exhibited little photolysis, indicating that phenol is stable under visible light. Under identical experimental conditions, the Bi_2S_3/Bi_2WO_6 composite exhibited much enhanced photocatalytic activity than both bare Bi_2WO_6 and Bi_2S_3. Bare Bi_2S_3 has negligible photocatalytic activity under visible-light irradiation, whereas the introduction of Bi_2S_3 into Bi_2WO_6 significantly enhances the photocatalytic activities of the composite. The photodegradation rate of phenol reached 51.6% in the presence of the Bi_2S_3/Bi_2WO_6 composite after 2 h of visible light irradiation, whereas only 12% of phenol was degraded by bare Bi_2WO_6 within the same time period, indicating that the Bi_2S_3/Bi_2WO_6 composite is a superior photocatalyst to bare Bi_2WO_6.

To quantitatively understand the reaction kinetics of phenol degradation in our experiments, we applied the Langmuir–Hinshelwood model, which is well-established for photocatalytic experiments when the concentration of the organic pollutant is in the millimolar range,[34] as expressed by

$$-\ln \frac{C}{C_0} = kt$$

where C_0 and C are the concentrations of pollutant in solution at time t_0 and t, respectively, and k is the apparent first-order rate constant. The apparent rate constant k is calculated to be 0.0010 and 0.0062 min^{-1} for bare Bi_2WO_6 and the Bi_2S_3/Bi_2WO_6 composite, respectively (Figure 5B). In other words, the photocatalytic activity of the Bi_2S_3/Bi_2WO_6 composite is about 6.2 times higher than that of bare Bi_2WO_6.

To further investigate the photodegradation of phenol, total organic carbon (TOC), which has been widely used to evaluate the degree of mineralization of organic species, was measured in the photodegradation process by the as-prepared samples under visible light, as shown in Figure 5C. The TOC removal efficiency of phenol reached 4.6% and 28.7% in the presence of bare Bi_2WO_6 and the Bi_2S_3/Bi_2WO_6 composite after 2 h of visible light irradiation, respectively, which confirmed that phenol could be mineralized by the as-prepared samples.

To approach the mechanism of the enhanced photocatalytic activity of the Bi_2S_3/Bi_2WO_6 composite, the relative band positions of the two semiconductors were investigated, since the band-edge potential levels play a crucial role in determining the flowchart of photoexcited charge carriers in a heterojunction. The conduction band (CB) bottoms (E_{CB}) were calculated empirically according to formula[35]

$$E_{CB} = X - 0.5E_g + E_0$$

where E_g is the band gap energy of the semiconductor, E_0 is scale factor relating the reference electrode redox level to the absolute vacuum scale (E_0 =−4.5 eV for normal hydrogen electrode), and X is the electronegativity of the semiconductor, which can be expressed as the geometric mean of the absolute electronegativity of the constituent atoms.[36] The X values for Bi_2WO_6 and Bi_2S_3 are calculated to be 6.36 and 5.95 eV, respectively, and the band gap energies of Bi_2WO_6 and Bi_2S_3 are 2.8 and 1.3 eV, respectively. Given the equation above, the conduction band bottom (E_{CB}) of Bi_2WO_6 and Bi_2S_3 is calculated to be 0.46 and 0.12 eV, respectively. Correspondingly, the valence band tops (E_{VB}) of Bi_2WO_6 and Bi_2S_3 are 3.26 and 1.42 eV, respectively. So the conduction band bottom (E_{CB}) of Bi_2S_3 is higher than that of Bi_2WO_6 and the valence band top (E_{VB}) of Bi_2S_3 is higher than that of Bi_2WO_6. The calculated results indicated the composite of Bi_2S_3/Bi_2WO_6 was advantageous for the separation and transportation of charge carriers. As illustrated in Figure 6, under visible-light irradiation,

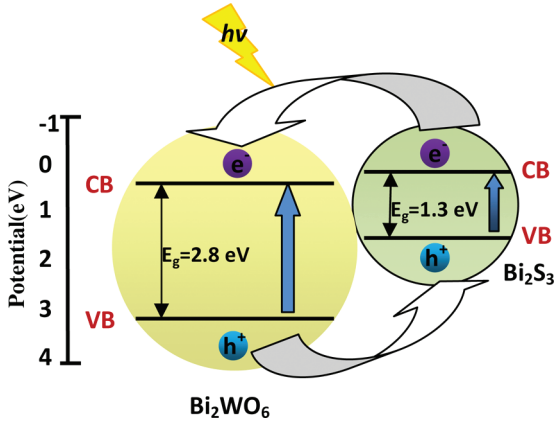

Figure 6. Diagram for energy band levels of Bi_2S_3/Bi_2WO_6 composites and the possible charge separation process.

both Bi_2S_3 and Bi_2WO_6 are easily excited and corresponding photoinduced electrons and holes are generated. Photogenerated electrons are injected with high efficiency from conduction band of Bi_2S_3 to conduction band of Bi_2WO_6 because of the intimate contact between the two semiconductors. Simultaneously, holes on the valence band of Bi_2WO_6 can be transferred to that of Bi_2S_3 under the band energy potential difference. In such a way, the photoinduced electrons and holes can be efficiently separated and the recombination of electron–hole pairs can be reduced, in accordance with the result of the PL spectra. Therefore, the Bi_2S_3/Bi_2WO_6 composite exhibits enhanced performance as compared to bare Bi_2WO_6 and Bi_2S_3.

CONCLUSION

In summary, Bi_2S_3/Bi_2WO_6 composite was prepared by a simple hydrothermal method in one step. The composite photocatalyst exhibits much enhanced photocatalytic activity in degradation of phenol under visible light irradiation, which is 6.2 times higher than that of bare Bi_2WO_6. On the basis of the calculated energy band positions, the mechanism of enhanced photocatalytic activity for the Bi_2S_3/Bi_2WO_6 composite was discussed. The enhanced activity is attributed to the effective separation of electron–holes pairs due to the formation of heterojunction between the two semiconductors. Such a composite photocatalyst is promising for water purification application and environmental remediation.

AUTHOR INFORMATION

Corresponding Author

*Tel.: +86-21-5241-5295. Fax: +86-21-5241-3122. E-mail: wzwang@mail.sic.ac.cn.

Notes

The authors declare no competing financial interest.

■ ACKNOWLEDGMENTS

We acknowledge the financial support from the National Natural Science Foundation of China (50972155, 50902144), National Basic Research Program of China (2010CB933503), and Science Foundation for Youth Scholar of State Key Laboratory of High Performance Ceramics and Superfine Microstructures (SKL 200904).

■ REFERENCES

(1) Hagfeldt, A.; Gratzel, M. *Chem. Rev.* **1995**, *95*, 49−68.
(2) Zou, Z. G.; Ye, J. H.; Sayama, K.; Arakawa, H. *Nature* **2001**, *414*, 625−627.
(3) Bao, N. Z.; Shen, L. M.; Takata, T.; Domen, K. *Chem. Mater.* **2008**, *20*, 110−117.
(4) Asahi, R.; Morikawa, T.; Ohwaki, T.; Aoki, K.; Taga, Y. *Science* **2001**, *293*, 269−271.
(5) Morales, W.; Cason, M.; Aina, O.; Tacconi, N. R.; Rajeshwar, K. *J. Am. Chem. Soc.* **2008**, *130*, 6318−6319.
(6) Wu, Q. P.; Li, D. Z.; Wu, L.; Wang, J.; Fu, X. Z.; Wang, X. X. *J. Mater. Chem.* **2006**, *16*, 1116−1117.
(7) Georgieva, J.; Armyanov, S.; Valova, E.; Poulios, I.; Sotiropoulos, S. *Electrochem. Commun.* **2007**, *9*, 365−370.
(8) Hou, Y.; Li, X. Y.; Zhao, Q. D.; Quan, X.; Chen, G. H. *Appl. Phys. Lett.* **2009**, *95*, 093108.
(9) Lianos, P. *J. Hazard. Mater.* **2011**, *185*, 575−590.
(10) Georgieva, J.; Valova, E.; Armyanov, S.; Philippidis, N.; Poulios, I.; Sotiropoulos, S. *J. Hazard. Mater.* **2011**, DOI: 10.1016/j.jhazmat.2011.11.069.
(11) Zhang, C.; Zhu, Y. F. *Chem. Mater.* **2005**, *17*, 3537−3545.
(12) Amano, F.; Yamakata, A.; Nogami, K.; Osawa, M.; Ohtani, B. *J. Am. Chem. Soc.* **2008**, *130*, 17650−17651.
(13) Liu, S. W.; Yu, J. G. *J. Solid State Chem.* **2008**, *181*, 1048−1055.
(14) Fu, H. B.; Zhang, L. W.; Yao, W. Q.; Zhu, Y. F. *Appl. Catal. B: Environ.* **2006**, *66*, 100−110.
(15) Li, G. S.; Zhang, D. Q.; Yu, J. C.; Leung, M. K. H. *Environ. Sci. Technol.* **2010**, *44*, 4276−4281.
(16) Wu, L.; Bi, J. H.; Li, Z. H.; Wang, X. X.; Fu, X. Z. *Catal. Today* **2008**, *131*, 15−20.
(17) Zhang, Z. J.; Wang, W. Z.; Shang, M.; Yin, W. Z. *J. Hazard. Mater.* **2010**, *177*, 1013−1018.
(18) Lee, M. K.; Shih, T. H. *J. Electrochem. Soc.* **2007**, *154*, 49−51.
(19) Wu, T.; Zhou, X. G.; Zhang, H.; Zhong, X. H. *Nano. Res.* **2010**, *3*, 379−386.
(20) Vogel, R.; Hoyer, P.; Weller, H. *J. Phys. Chem.* **1994**, *98*, 3183−3188.
(21) Bessekhouad, Y.; Mohammedi, M.; Trari, M. *Sol. Energy Mater. Sol. Cells* **2002**, *73*, 339−350.
(22) Bao, H.; Li, C. M.; Cui, X. Q.; Gan, Y.; Song, Q. L.; Guo, J. *Small* **2008**, *4*, 1125−1129.
(23) Zhang, B.; Ye, X. C.; Hou, W. Y.; Zhao, Y.; Xie, Y. *J. Phys. Chem. B* **2006**, *110*, 8978−8985.
(24) Cademartiri, L.; Scotognella, F.; O'Brien, P. G.; Lotsch, B. V.; Thomson, J.; Petrov, S.; Kherani, N. P.; Ozin, G. A. *Nano Lett.* **2009**, *9*, 1482−1486.
(25) Rabin, O.; Perez, J. M.; Grimm, J.; Wojtkiewicz, G.; Weissleder, R. *Nat. Mater.* **2006**, *5*, 118−122.
(26) Yao, K.; Gong, W. W.; Hu, Y. F.; Liang, X. L.; Chen, Q.; Peng, L. M. *J. Phys. Chem. C* **2008**, *112*, 8721−8724.
(27) Robert, D. *Catal. Today* **2007**, *122*, 20−26.
(28) Bessekhouad, Y.; Robert, D.; Weber, J. V. *J. Photochem. Photobiol. A: Chem.* **2004**, *163*, 569−580.
(29) Zhang, Z. J.; Wang, W. Z.; Gao, E. P.; Shang, M.; Xu, J. H. *J. Hazard. Mater.* **2011**, *196*, 255−262.
(30) Zhang, Z. J.; Wang, W. Z.; Yin, W. Z.; Shang, M.; Wang, L.; Sun, S. M. *Appl. Catal. B: Environ.* **2010**, *101*, 68−73.
(31) Tang, J. W.; Zou, Z. G.; Ye, J. H. *J. Phys. Chem. B* **2003**, *107*, 14265−14269.
(32) Fujihara, K.; Izumi, S.; Ohno, T.; Matsumura, M. *J. Photochem. Photobiol. A: Chem.* **2000**, *132*, 99−104.
(33) Xiao, Q.; Zhang, J.; Xiao, C.; Tan, X. K. *Catal. Commun.* **2008**, *9*, 1247−1253.
(34) Sakkas, V. A.; Arabatzis, I. M.; Konstantinou, I. K.; Dimou, A. D.; Albanis, T. A.; Falaras, P. *Appl. Catal. B: Environ.* **2004**, *49*, 195−205.
(35) Lv, J.; Kako, T.; Zou, Z. G.; Ye, J. H. *Appl. Phys. Lett.* **2009**, *95*, 032107.
(36) Xu, Y.; Schoonen, M. A. A. *Am. Mineral.* **2000**, *85*, 543−556.